AN ELECTROCHEMICAL IMPEDANCE SPECTROSCOPY AND POTENTIODYNAMIC POLARIZATION STUDY OF THE EFFECT OF UNIDIRECTIONAL ROUGHNESS ON THE CORROSION OF NICKEL

A. S. TOLOEI, V. STOILOV & D. O. NORTHWOOD
Department of Mechanical, Automotive and Materials Engineering, University of Windsor, Canada.

ABSTRACT

The effect of unidirectional surface roughness on the corrosion behaviour of nickel in 0.5 M H_2SO_4 solution was investigated using electrochemical impedance spectroscopy and potentiodynamic polarization techniques. The surfaces, both before and after corrosion, were characterized by scanning electron microscopy, profilometry for roughness and energy dispersive spectroscopy for oxygen content. The results were compared with those for patterned samples consisting of an array of holes. For the unidirectional surface roughness samples, an increase in roughness gave rise to an increase in corrosion rate, reflecting the decreased ability to form a stable passive film. The patterned samples showed a higher corrosion resistance, which is attributed to a different corrosion protection mechanism, namely heterogeneous wetting.

Keywords: Corrosion, nickel, passive layer, patterned surface, unidirectional roughness.

1 INTRODUCTION

The corrosion of nickel in different electrolytes has been the subject of numerous studies due to the high technological importance of Ni and Ni-base alloys[1]. With respect to the corrosion mechanisms in acids, in particular H_2SO_4, Gilli *et al.* [2] and De Gromoboy and Shreir [3] have shown that the initial step in the corrosion of nickel in sulphuric acid is the formation of an unstable adsorbed intermediate, NiOH, as shown in the following equation:

$$Ni + H_2O \rightarrow NiOH + H^+ + e^- \qquad (1)$$

NiOH can then react in two different ways. If oxidation of NiOH leads to Ni^{2+}, there is no passivation of the metal, but rather active corrosion of Ni according to eqn (2):

$$NiOH + H^+ \rightarrow Ni^{2+} + e^- + H_2O \qquad (2)$$

However, if oxidation of the intermediate leads to NiO formation, there can be passivation of the Ni as shown in eqn (3):

$$NiOH \rightarrow NiO + H^+ + e^- \qquad (3)$$

The surface NiO film constitutes only the first step in passivation. By polarization of the electrode towards more positive potential values, higher oxides of Ni can be formed. The presence of NiO_x imparts stable passivity to the metal. Gilli *et al.* [2], consider that the formation of a passive film on nickel surface to be the main reason for the good corrosion resistance of nickel.

There are different methods to protect nickel against corrosion in acidic media such as using inhibitors and surface modification [4]. Typically, the general and localized corrosion behaviour of alloys depends on their roughness and passivation behaviour. The effect of surface roughness has been investigated on both localized and general corrosion of different metals such as stainless steel, copper, aluminium, magnesium, titanium and mild steel [5–10].

In all cases, except for AE44 Mg-alloy [5] and mild steel [6], an increase in surface roughness led to an increase in both the general corrosion rate and pitting degradation. However, to the authors' best knowledge, there is no published data on the effect of surface roughness on the corrosion behaviour of nickel in H_2SO_4 solution.

In this research, the effect of the level of unidirectional roughness on the corrosion behaviour of nickel in 0.5 M H_2SO_4 solution has been investigated using potentiodynamic polarization and electrochemical impedance spectroscopy techniques. Some preliminary results have been presented in Toloei *et al.* [11]. The results are compared with our results on the effect of surface patterning on the corrosion of nickel in the same electrolyte [12-14].

2 EXPERIMENTAL PROCEDURE

The nickel samples were mechanically wet-ground using silicon carbide papers with different grit sizes (G60 to G1200). The grinding was performed in a manner that produced unidirectional roughness. The surface patterned samples consisted of an array of holes of various diameters (D) and inter-hole spacings (L) that were produced by a laser ablation process [12]. The comparative specimens used in this study were D10L20 and D20L20. The dimensions are in microns.

Electrochemical measurements were carried out with a CHI 660D Electrochemical Workstation Beta (Chen Hua, Shanghai) in a standard three-electrode cell consisting of the nickel sample as the working electrode, a saturated calomel electrode as the reference electrode and a platinum wire counter electrode. All measurements were made at room temperature in a naturally aerated 0.5 M H_2SO_4 solution. For the potentiodynamic polarization tests, samples were given 30 min in order to reach a relatively stable open circuit potential (OCP) before carrying out the testing. For the electrochemical impedance spectroscopy measurements, the impedance was measured at frequencies between 10^{-2} and 10^4 Hz in order to ensure a complete characterization of the electrode/electrolyte interface and corresponding processes. All the Nyquist plots were analysed by fitting the experimental data to an equivalent circuit model. The model chosen for the fitting was a commonly used model for Nickel [4] (Fig. 1). In this circuit, R_s represents the solution resistance; R_{ct} is the charge transfer resistance and CPE is the constant phase element related to the double-layer capacitance. The impedance, Z, of CPE is calculated from eqn (4):

$$Z_{CPE} = [Q(j\omega)]^{-n} \qquad (4)$$

Two values, Q and n, define the CPE. Q is the CPE constant, which is a combination of properties related to the surface and electro-active species, $j^2 = -1$ the imaginary number, the angular frequency and n is a CPE exponent that can be used as a measure of the heterogeneity or roughness of the surface.

Scanning electron microscopy (SEM), energy dispersive spectroscopy (EDS) and profilometry (Wyko Surface Profiling System NT-1100) were used to characterize the surface and measure the average surface roughness (R_a), root-mean-squared roughness (R_q) and the average of the 10 greatest peak-to-valley separations (R_z) both before and after corrosion testing.
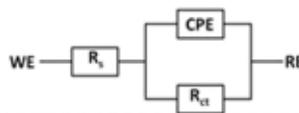
Figure 1: Equivalent circuit model.

3 RESULTS

3.1 SEM analysis

Figure 2 presents SEM micrographs of two of the unidirectional roughness samples (G60 and G800) and one patterned sample (D10L20) both before and after corrosion. Looking at the SEM micrographs for G60 (Fig. 2a and b), we can readily see that corrosion has taken place over the total sample surface but that evidence of the grooves (from the unidirectional grinding) is retained, albeit at a somewhat larger scale. The corrosion seems to be concentrated along the grooves. For the G800 sample (Fig. 2c and d), the grooves are much finer and are much less obvious after corrosion. However, there is evidence of heavy corrosion along what is presumed to be one of the deeper grooves formed on the initial unidirectional grinding. These observations are in agreement with Lee *et al.*'s [15] finding that samples with deep grooves, i.e. those with higher reduced valley depth (R_{vk}) values, show poorer corrosion resistance and Suter *et al.*'s [9] observations that these deeper grooves trap the corrosive ions and corrosion products leading to more pitting.

By contrast, the patterned sample (D10L20) (Fig. 2e and f), showed little change in appearance after corrosion testing. The reasons for this difference in behaviour compared with the unidirectional ground samples is related to a heterogeneous wetting process taking place in some patterned samples as described in detail by Toloei *et al*. [13].
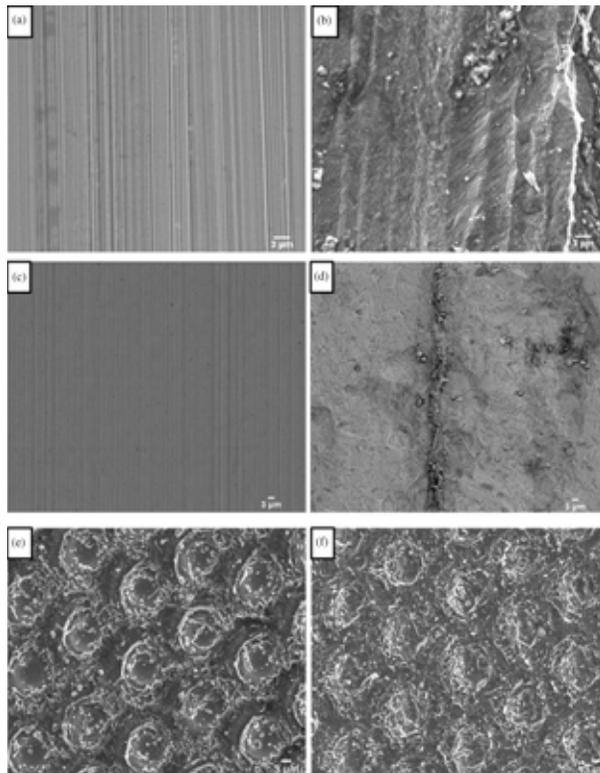
Figure 2: SEM micrographs of samples. G60: (a) before corrosion, (b) after corrosion; G800: (c) before corrosion, (d) after corrosion; and D10L20: (e) before corrosion and (f) after corrosion.

3.2 Roughness measurements

Figure 3 shows the average roughness (R_a) values of all unidirectionally ground samples and two patterned samples both before and after corrosion testing. R_a (before corrosion) decreases systematically with increasing grit number from G60 to G1200. R_a (before corrosion) for the patterned samples are higher than the unidirectionally ground samples. This is because of the micron-sized holes and molten metal splashes created close to the holes during the laser ablation fabrication. For all G60 to G1200 samples, the R_a values significantly increased after corrosion. This is in agreement with the findings of Hamed *et al.* [16] for the corrosion of Ni in H_2SO_4 solution. The changes in roughness for the patterned samples were relatively quite small and confirm the SEM observations (Fig. 2e and f), that indicate limited corrosion. Similar results to those for R_a have been found for R_q (root-mean-squared roughness) and R_z (average of the 10 greatest peak-to-valley separations).

3.3 Potentiodynamic polarization measurements

A typical potentiodynamic polarization curve obtained at increasing potential for nickel immersed in 0.5 M H_2SO_4 is shown in Fig. 4. As can be seen, there are three different regions, namely active, passive and transpassive. In the active region, the corrosion increases. In the passive region, it decreases and reaches an approximately constant value before reaching the pitting potential. Finally, as a result of the removal of any passive layer, the metal goes to transpassive region and corrosion rate increases.

Selected polarization curves of nickel samples with different surface roughness are shown in Fig. 5. There was no significant difference in the cathodic branch of the polarization curves for samples with different surface roughnesses. This suggests that any corrosion rate changes were solely due to the anodic behaviour of the sample. As can be seen in Fig. 5, the passive
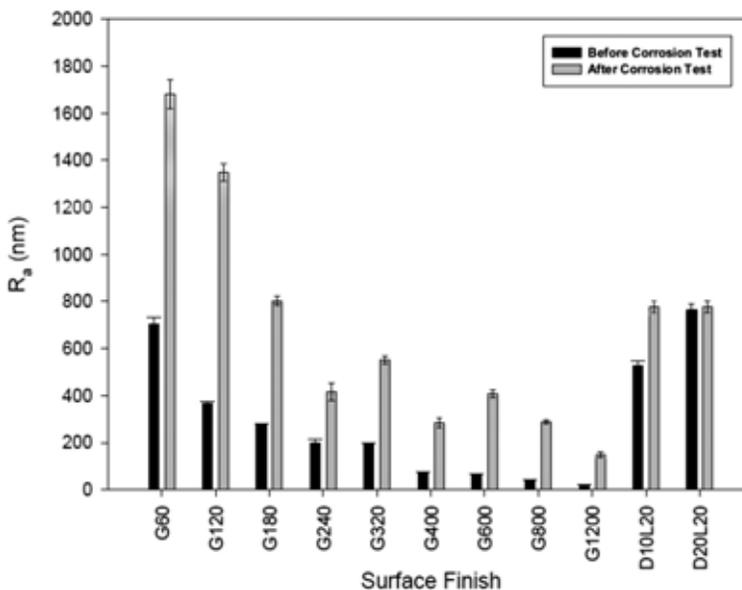
Figure 3: R_a values for different surface finishes before and after corrosion testing.
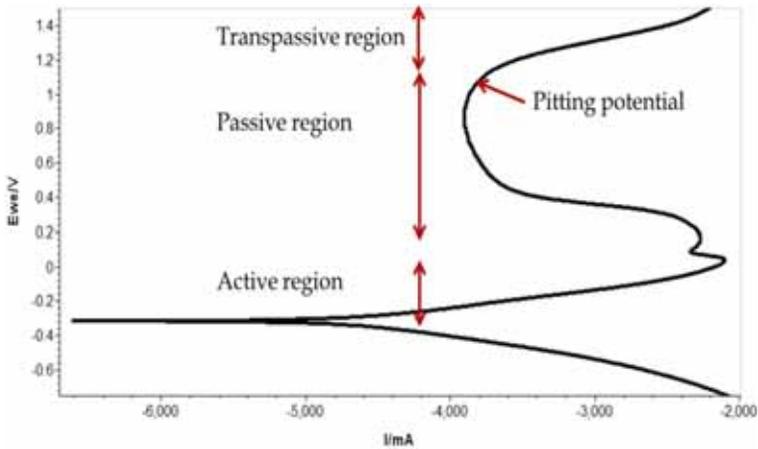
Figure 4: Typical polarization curves for Ni in 0.5M H_2SO_4.
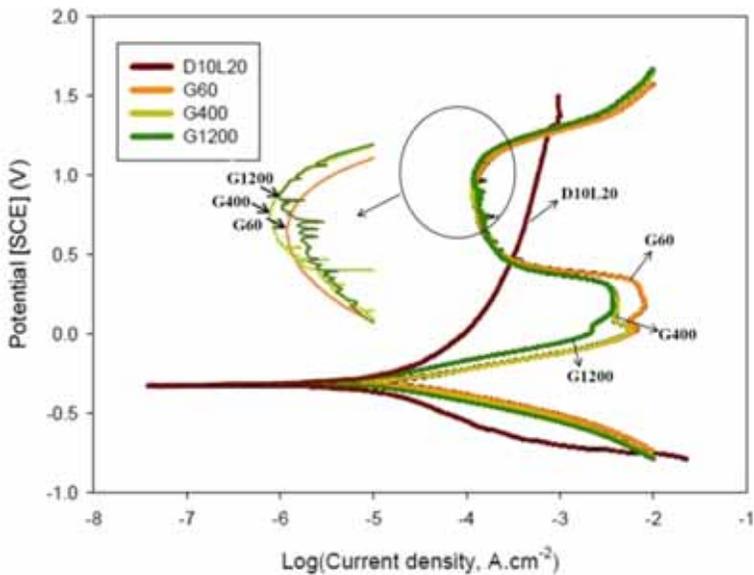
Figure 5: Polarization curves for samples G60, G400, G1200 and D10L20.

layer breakdown potential increased with decreasing surface roughness from sample G60 to G1200, which is an indication of a higher pitting resistance [9].

The electrochemical corrosion parameters obtained from all polarization curves are listed in Table 1. P_i, the corrosion rate, has been calculated in mils per year (mpy) from i_{corr} using eqn (5):

$$P_i = K\,(i_{corr})EW/\rho \qquad (5)$$

where K is the constant for converting units, i_{corr} the corrosion current density ($\mu A/cm^2$), ρ the alloy density (g/cm^3) and EW the alloy equivalent weight (g/equivalent). A cursory

examination of Table 1 indicates that the corrosion rate decreases with increasing grit size, i.e. smoother surfaces are more corrosion resistant. The patterned samples, however, are more corrosion resistant than the smoothest ground samples. This will be examined further in the discussion section.

Table 1: Corrosion parameters obtained from dynamic polarization measurements.

Sample	E_{corr} (mV)	β_a (mV)	β_c (mV)	i_{corr} ($\mu A/cm^2$)	R_p (Ω/cm^2)	P_i (mil/year)
G60	–319	104.7	114.6	21.93	1086	9.53
G120	–321.8	109.5	118.3	21.64	1144	9.40
G180	–325.5	111.2	113.8	19.22	1275	8.35
G240	–310.5	110.0	116.8	19.27	1275	8.37
G320	–300.8	100.0	112.1	18.32	1255	7.96
G400	–313.9	112.1	113.3	17.26	1419	7.50
G600	–312.6	123.8	111.1	14.67	1735	6.37
G800	–272.9	82.3	107.9	12.60	1614	5.48
G1200	–272.7	120.3	105.3	8.43	2899	3.66
D10L20	–327.4	153.4	128.5	6.01	5046	2.61
D20L20	–303.3	132.6	173.3	1.16	28070	0.50

3.4 EIS results

Figure 6 presents the Nyquist diagrams for the different surface roughnesses. The diagrams consist of a large capacitive loop at high frequency (HF). The HF capacitive loop is related to the charge transfer process in metal corrosion and the double-layer behaviour at the film/solution interface. The semicircle diameter increases with decreasing roughness, indicating that the corrosion is mainly a charge transfer process [17], which results in a higher R_{ct} value. The patterned sample (D10L20) has the largest capacitive loop reflecting the highest R_{ct} value.
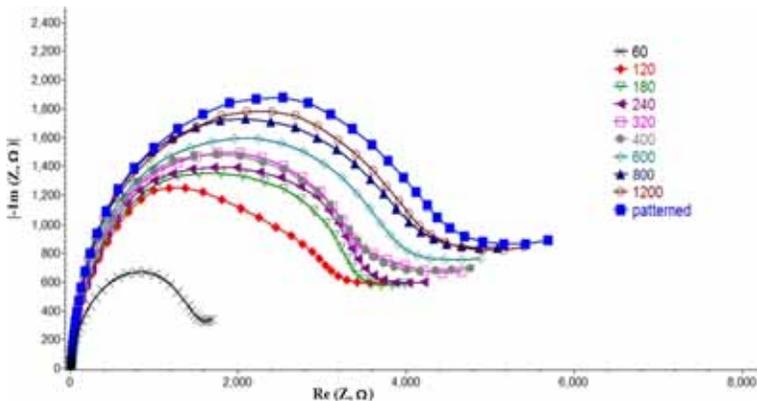
Figure 6: Nyquist diagrams for Ni with different roughnesses.

Figure 7 shows the Bode and Bode phase plots for one of the samples (G60). The Bode plot shows only one phase maximum at intermediate frequencies. This result indicates that the corrosion process occurs via a one-step process corresponding to one time constant. The maximum phase angle θ_{max} is also less than 80°, which is considered to be a result of the roughness of the electrode surface [16].

All data were curve-fitted and analysed using an EIS spectrum analyser. A combination of randomize followed by the most widely used optimization algorithm, Levenberg-Marquardt fitting, was used to fit the results [18]. A good fit was observed between the experimental data and the simulated values as can be seen in Fig. 7 for the Bode plots. The values of the equivalent circuit elements for the corrosion of nickel for various surface roughnesses are summarized in Table 2. The different values obtained for the n and CPE exponent can be related to the roughness of the surface of nickel [19]. The rougher the samples, the lower the n value and the higher the CPE values.

According to Table 2, the values of R_{ct} and (n) increased generally from sample G60 to G1200. R_{ct} is a measure of electron transfer across the surface and inversely proportional to the corrosion rate [20]. The decrease in the CPE value or increase in n value can be attributed to the formation of passive layer at the metal surface [20].
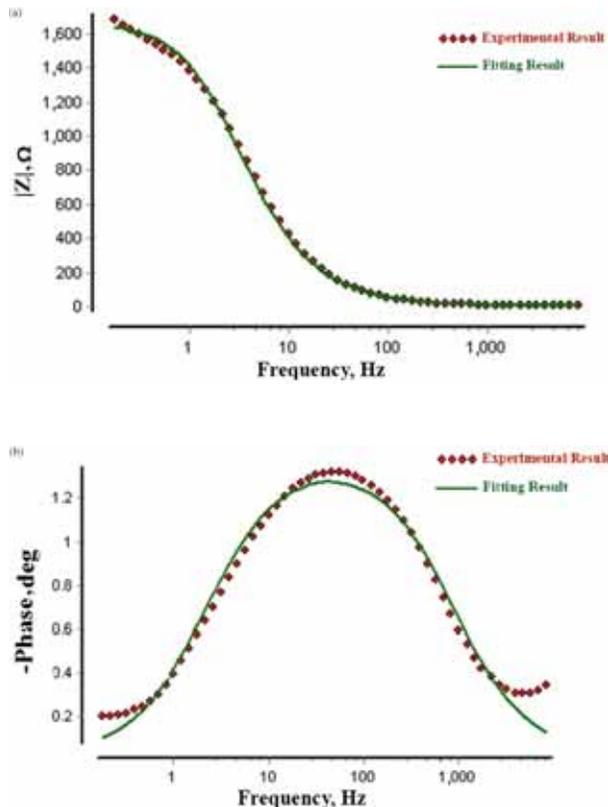
Figure 7: (a) Bode magnitude and (b) Bode phase plots for fitted and experimental results for sample G60.

Table 2: Equivalent circuit elements for various surface roughnesses.

Sample	R_s (Ω cm^2)	R_{ct} (Ω cm^2)	CPE (Ω^{-1} cm^{-2} S^n)	n
G60	7.99	1664.2	5.58×10^{-5}	0.898
G120	8.46	3220.5	4.73×10^{-5}	0.916
G180	9.21	3514.7	3.76×10^{-5}	0.922
G240	9.01	3655.7	4.51×10^{-5}	0.921
G320	8.56	3764	4.51×10^{-5}	0.920
G400	8.84	3838.4	4.56×10^{-5}	0.920
G600	8.32	4114.9	4.03×10^{-5}	0.922
G800	8.68	4463.1	4.57×10^{-5}	0.921
G1200	8.56	4498.7	4.73×10^{-5}	0.923
D10L20	8.98	4733.5	4.52×10^{-5}	0.922

3.5 EDS analysis

EDS was used to measure the changes in oxygen concentration on the surface of the samples before and after corrosion testing and the results are summarized in Table 3. All samples, except the patterned ones, had similar oxygen contents before corrosion testing but the oxygen content increased for all samples after corrosion. Looking at the oxygen content increase of the surface, the largest increases were for the two roughest samples (G60 and G120). For intermediate roughness samples (G180–G400) there was a much smaller increase in oxygen content. For the smoothest samples (G600–G1200), the increase in oxygen content stabilized at about 2.2 wt% O. As demonstrated from the electrochemical results, G60 and G120 exhibited the highest corrosion rates, and the corrosion rate decreased with decreasing roughness. For samples G600–G1200, where the final oxygen content was ~3.7wt% O, this could be indicative of the formation of a stable passive film as suggested by Suter *et al*. [9] for high purity aluminum.

4 DISCUSSION

4.1 Relationship between corrosion rate and roughness

Figures 8–10 illustrate the relationship between the corrosion rate (P_i in Table 1) as determined by potentiodynamic polarization tests and the roughness values: R_a in Fig. 8, R_q in Fig. 9 and R_z in Fig. 10. All the three plots show the same general trends. First, an increase in roughness leads to an increase in corrosion rate. As noted in the Introduction, this is a general trend seen for corrosion of metals that form a protective passive film [9]. Looking at the general shape of the plot, we can see that any deviation from a perfectly flat surface dramatically increases the corrosion rate. The rate of change of corrosion rate with roughness then decreases and, for the highest roughness values, the corrosion rate appears to reach a plateau. A similar behaviour was reported by Li and Li [8] for Cu in a 3.5% NaCl solution. The other point of interest in Figs 8–10 is that the patterned samples show much lower corrosion rates than unidirectional roughness samples with equivalent, or much lower, roughness. This strongly suggests a different corrosion protection mechanism for the patterned samples.

Table 3: Oxygen contents on the surface of the samples before and after corrosion testing.

Sample	SiC particle size (μm)	Oxygen wt% before corrosion	Oxygen wt% after corrosion	Oxygen wt% difference
G60	254	1.17	4.60	3.43
G120	102	1.37	4.71	3.34
G180	80	1.19	2.07	0.88
G240	60	1.20	2.6	1.40
G320	40	1.18	2.52	1.34
G400	30	1.20	2.11	0.91
G600	15	1.48	3.69	2.21
G800	13	1.54	3.69	2.15
G1200	9	1.49	3.75	2.26
D10L20 (outside the hole)	-	2.2	2.5	0.3
D10L20 (inside the hole)	-	2.2	4.2	2
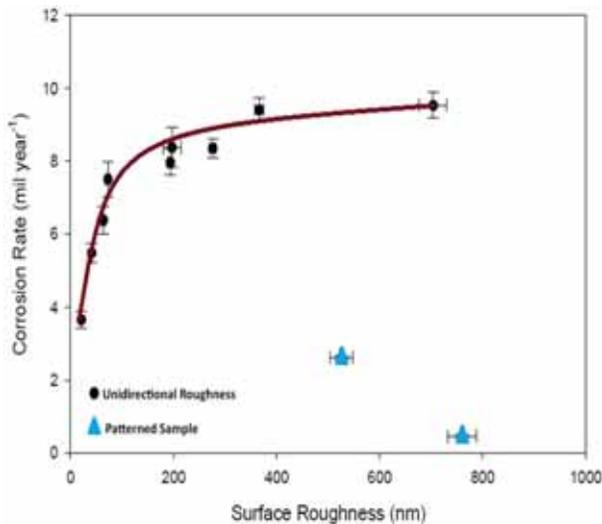
Figure 8: Dependence of corrosion rate on average surface roughness (Ra) for surfaces with unidirectional roughness and patterned samples.

In addition to potentiodynamic polarization results, we have the EIS results. One measure of corrosion resistance in the EIS studies is R_{ct}, the charge transfer resistance. Figure 11 is a plot of R_{ct} vs. R_a, the average surface roughness. Also plotted in Fig. 11 is R_p, the polarization resistance obtained from the potentiodynamic polarization tests. The EIS results show the same trend, namely decreasing R_{ct}, i.e. increasing corrosion rate, with increasing roughness. A similar trend in R_p vs. roughness has been reported by Lee *et al*. [15] for 21 Cr ferritic stainless steel in a 1 M NaCl solution. This study was also for a unidirectional type of roughness.
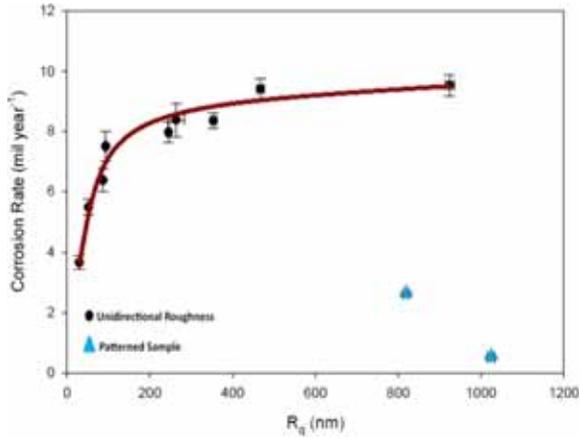
Figure 9: Dependence of corrosion rate on R_q for surfaces with unidirectional roughness and patterned samples.
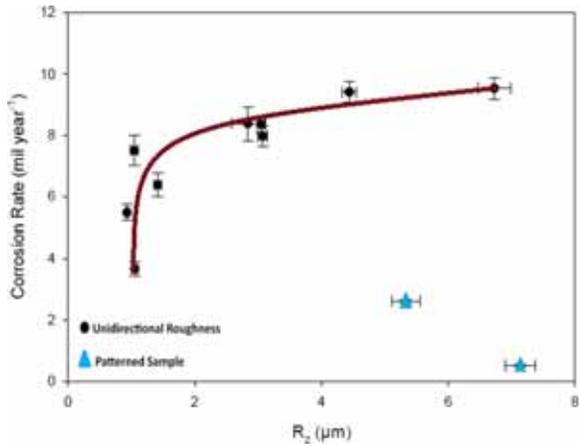
Figure 10: Dependence of corrosion rate on R_z for surfaces with unidirectional roughness and patterned samples.

4.2 Corrosion mechanisms

The electrochemical results clearly demonstrate that an increase in unidirectional surface roughness leads to a commensurate decrease in R_p and R_{ct} and, therefore, an increase in corrosion rate. In the rougher samples, there is more contact area between the corrosive medium and the metal (Ni). There is also trapping of the corrosive ions in the deep grooves, leading to an autocatalytic process such as pitting [21]. Both of these factors would lead to an increased corrosion rate. This is also consistent with Li and Li [8] who measured the electron work function (EWF) of Cu and found that the EWF decreased with increasing roughness. A rougher surface, therefore, could more readily release electrons that would result in a higher corrosion rate. There is another important observation related to mechanisms and that is the EDS results for oxygen content on the surface after corrosion. The results for G600 to G1200 suggest the formation of a stable passive film. Such a passive film would provide better corrosion protection, as evidenced by these samples showing the lowest corrosion rates for
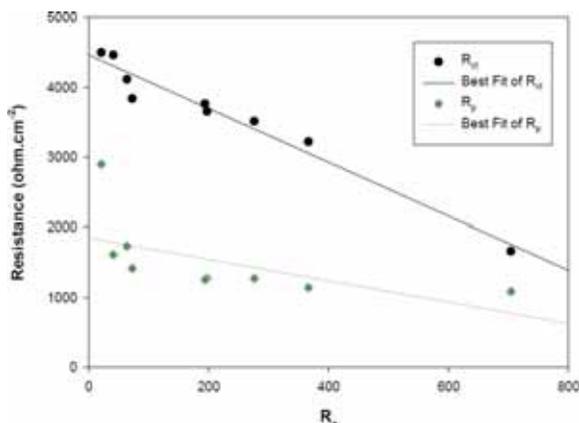
Figure 11: The effect of roughness on R_p and R_{ct}.

the unidirectional roughness samples. In the patterned samples, as we have discussed before in Toloei *et al*. [13], there is a different mechanism and heterogeneous wetting decreases the surface area exposed to the sulphuric acid solution, thus reducing the corrosion rate.

5 CONCLUSIONS

Both potentiodynamic polarization and EIS measurements for the corrosion in 0.5 M H_2SO_4 solution of nickel samples with varying levels of unidirectional roughness show that the corrosion rate increases with roughness (R_a, R_q, R_z). A low surface roughness promotes the formation of a stable passive film. For the higher roughness samples, there is a greater contact area between the corrosive medium and metal together with trapping of corrosive ions in the deep grooves leading to processes such as pitting. In all instances, there was an increase in roughness after corrosion.

For patterned samples, consisting of an array of holes, the change in roughness after corrosion testing was much less than for the unidirectional roughness samples, as were the corrosion rates. The corrosion protection offered by the patterned surface is attributed to heterogeneous wetting, which reduces the surface area of the nickel that is exposed to the sulphuric acid solution.

REFERENCES

[1] Marcus, P. & Oudar, J., *Corrosion Mechanisms in Theory and Practice*, 1st edn., Marcel Dekker: New York, 1995.

[2] Gilli, G., Borea, P., Zucchi, F. & Trabanelli, G., Passivation of Ni caused by layers of salts in concentrated H_2SO_4. *Corrosion Science*, **9(9)**, pp. 673–681, 1969. doi: http://dx.doi.org/10.1016/S0010-938X(69)80098-3

[3] De Gromoboy, T.S. & Shreir, L.L., The formation of nickel oxides during the passivation of nickel in relation to the potential/ph diagram. *Electrochimica Acta*, **11(7)**, pp. 895–904, 1966. doi: http://dx.doi.org/10.1016/0013-4686(66)87066-4

[4] Said, F., Souissi, N., Dermaj, A., Hajjaji, N., Triki, E. & Srhiri, A., Effect of (r+, x−) salts addition on nickel corrosion in 1 M sulfuric acid medium. *Materials and Corrosion*, **56(9)**, pp. 619–623, 2005. doi: http://dx.doi.org/10.1002/maco.200503863

[5] Alvarez, R.B., Martin, H.J., Horstemeyer, M.F., Chandler, M.Q., Williams, N., Wang, P.T. & Ruiz, A., Corrosion relationships as a function of time and surface roughness on a structural AE44 magnesium alloy. *Corrosion Science*, **52(5)**, pp. 1635–1648, 2010. doi: http://dx.doi.org/10.1016/j.corsci.2010.01.018

[6]   Abosrra, L., Ashour, A.F., Mitchell, S.C. & Youseffi, M., Corrosion of mild steel and 316L austenitic stainless steel with different surface roughness in sodium chloride saline solutions. *WIT Transactions on Engineering Sciences*, **65**, pp. 161–172, 2009. doi: http://dx.doi.org/10.2495/ECOR090161

[7]   Cabrini, M., Cigada, A., Rondell, G. & Vicentini, B., Effect of different surface finishing and of hydroxyapatite coatings on passive and corrosion current of Ti6Al4V alloy in simulated physiological solution. *Biomaterials*, **18(11)**, pp. 783–787, 1997. doi: http://dx.doi.org/10.1016/S0142-9612(96)00205-0

[8]   Li, W., & Li, D.Y., Influence of surface morphology on corrosion and electronic behavior. *Acta Materialia*, **54(2)**, pp. 445–452, 2006. doi: http://dx.doi.org/10.1016/j.actamat.2005.09.017

[9]   Suter, T., Müller, Y., Schmutz, P. & von Trzebiatowski, O., Microelectrochemical studies of pit initiation on high purity and ultra high purity aluminum. *Advanced Engineering Materials*, **7(5)**, pp. 339–348, 2005. doi: http://dx.doi.org/10.1002/adem.200500067

[10] Walter, R. & Kannan, M.B., Influence of surface roughness on the corrosion behaviour of magnesium alloy. *Materials & Design*, **32(4)**, pp. 2350–2354, 2011. doi: http://dx.doi.org/10.1016/j.matdes.2010.12.016

[11] Toloei, A.S., Stoilov, V. & Northwood, D.O., The effect of different surface topographies on the corrosion behaviour of nickel. *WIT Transactions on Engineering Sciences*, **77**, pp. 193–204, 2013. doi: http://dx.doi.org/10.2495/MC130171

[12] Bigdeli Karimi, M., Stoilov, V. & Northwood, D.O., Improving corrosion performance by surface patterning. *WIT Transactions on Engineering Sciences*, **72**, pp. 85–93, 2011. doi: http://dx.doi.org/10.2495/MC110081

[13] Toloei, A.S., Stoilov, V. & Northwood, D.O., A new approach to combating corrosion of metallic materials. *Applied Surface Science*, **284**, pp. 242–247, 2013. doi: http://dx.doi.org/10.1016/j.apsusc.2013.07.088

[14] Toloei, A., Stoilov, V. & Northwood, D.O., The effect of creating different size surface patterns on corrosion properties of nickel. *Proc of ASME International Mechanical Engineering Congress & Exposition (IMECE2012-89407)*, pp. 1297–1303, Houston, USA, 2012.

[15] Lee, S.M., Lee, W.G., Kim, Y.H. & Jang, H,, Surface roughness and the corrosion resistance of 21Cr ferritic stainless steel. *Corrosion Science*, **63**, pp. 404–409, 2012. doi: http://dx.doi.org/10.1016/j.corsci.2012.06.031

[16] Hamed, E., Abd El-Rehim, S.S., El-Shahat, M.F. & Shaltot, A.M., Corrosion inhibition of nickel in H_2SO_4 solution by alanine. *Materials Science and Engineering: B*, **177(5)**, pp. 441–448, 2012. doi: http://dx.doi.org/10.1016/j.mseb.2012.01.016

[17] Bentiss, F., Lagrenee, M., Traisnel, M. & Hornez, J.C., The corrosion inhibition of mild steel in acidic media by a new triazole derivative. *Corrosion Science*, **41(4)**, pp. 789–803, 1999. doi: http://dx.doi.org/10.1016/S0010-938X(98)00153-X

[18] Nocedal, J. & Wright, S.J., *Numerical Optimization*, 1st edn, Springer: USA, 1999. doi: http://dx.doi.org/10.1007/b98874

[19] Gregori, J., García-Jareño, J.J., Giménez-Romero, D. & Vicente, F., Kinetic calculations of the Ni anodic dissolution from EIS. *Journal of Solid State Electrochemistry*, **9(2)**, pp. 83–90, 2005. doi: http://dx.doi.org/10.1007/s10008-004-0557-2

[20] Abd-El-Nabey, B.A., Abdel-Gaber, A.M., Said Ali, M.E., Khamis, E. & El-Housseiny, S., Cannabis plant extract as inhibitor for the corrosion of nickel in 0.5 M H_2SO_4. *International Journal of Electrochemical Science*, **7**, pp. 11811–11826, 2012.

[21] Punckt, C., Bolscher, M., Rotermund, H.H., Mikhailov, A.S., Organ, L., Budiansky, N., Scully, J.R. & Hudson, J.L., Sudden onset of pitting corrosion on stainless steel as a critical phenomenon. *Science*, **305**, pp. 1133–1136, 2004. doi: http://dx.doi.org/10.1126/science.1101358